JOURNAL OF GEOPHYSICAL RESEARCH, VOL. 113, D14104, doi:10.1029/2007JD009289, 2008

Intermediate-scale tropical inertia gravity waves observed during the TWP-ICE campaign

S. Evan[1] and M. J. Alexander[2]

Received 17 August 2007; revised 25 January 2008; accepted 22 February 2008; published 16 July 2008.

[1] We describe a 2-day wave event observed in high-resolution radiosonde soundings of horizontal wind and temperature taken during the TWP-ICE experiment in Darwin area. The vertical profiles of temperature, zonal and meridional wind speeds are analyzed using the S-transform wavelet analysis. Results of the analysis reveal the presence of 2-day inertia gravity waves in the stratosphere between 20 and 27 km. The wave presents vertical and horizontal wavelengths of around 6 km and 7220 km respectively. The wave was observed to propagate southeastward during the end of the easterly phase of the QBO. The total vertical momentum flux associated with the waves is estimated to be 1 to 2.2×10^{-3} m^2s^{-2}. This is of the same order of magnitude as previous observations of 4–10 day Kelvin waves in the lower stratosphere.

Citation: Evan, S., and M. J. Alexander (2008), Intermediate-scale tropical inertia gravity waves observed during the TWP-ICE campaign, *J. Geophys. Res.*, *113*, D14104, doi:10.1029/2007JD009289.

1. Introduction

[2] Tropical convection can excite a broad spectrum of waves, from planetary-scale Kelvin waves, synoptic-scale Rossby-gravity and inertia-gravity waves, down to mesoscale gravity waves. These vertically propagating waves from the troposphere play an important role in the dynamics of the tropical middle atmosphere. By depositing horizontal momentum they provide the necessary forcing to drive the quasi-biennal oscillation (QBO) in the stratosphere and the semiannual oscillation (SAO) in the upper stratosphere and mesosphere. This process is referred to as the wave-mean flow interaction in which the background flow acts as a filter on the propagation of the waves and in return the momentum fluxes due to the waves have an effect on the background flow [*Plumb*, 1984].

[3] Although Kelvin waves and Rossby-gravity waves provide a major contribution to the vertical flux of momentum needed to drive the QBO, *Dunkerton* [1997] has demonstrated that additional wave flux from internal gravity waves is required to generate a realistic QBO in the models.

[4] *Sassi and Garcia* [1997] investigated the role of equatorial waves forced by convection in the SAO by means of numerical simulations with a three-dimensional quasi-nonlinear equatorial β-plane model. Results of the simulations suggest that the forcing in the upper stratosphere is predominantly due to planetary-scale Kelvin waves. However, they demonstrated that in the mesosphere the SAO can be driven mainly by intermediate-scale Kelvin and inertia-gravity waves (zonal wave number k = 4–15) and that the contribution from Kelvin waves (zonal wave number k = 1–3) is negligible. *Antonita et al.* [2007] quantified the contribution of gravity waves toward forcing of the stratospheric SAO. The waves they observed in temperature measurements over Gadanki (13.5°N, 79.2°E) and Trivandrum (8.5°N, 76.9°E) from November 2002 to June 2005 contributed to 30–50% of the observed acceleration during the evolution of the westerly phase of the stratospheric SAO.

[5] *Lieberman et al.* [2006] obtained observational evidence for diurnal intermediate-scale inertia-gravity waves in the mesosphere and lower thermosphere. They have shown that an inverse relationship exists between inertia-gravity wave variance (wave numbers 9–17) and the wind magnitude.

[6] These different studies suggest that planetary scale waves alone cannot explain the dominant circulation patterns in the stratosphere and mesosphere. Mesoscale gravity waves and intermediate-scale inertia-gravity waves can have an important role in the dynamics of this region. As their role is not well known, it is necessary to better understand from observations the morphology of such waves and their contribution to the driving of the tropical middle atmosphere circulation. In particular, data from previous campaigns in different tropical regions have been analyzed to assess the properties of intermediate-scale inertia-gravity waves.

[7] A pioneering study of equatorial inertia-gravity waves was made by *Cadet and Teitelbaum* [1979]. On the basis of radiosoundings collected over the Atlantic Ocean, they revealed inertia-gravity waves with a period of 35 h, a zonal wavelength of 2400 km and a vertical wavelength of 5 km. The waves showed a westward and upward propagation during the easterly shear phase of the QBO.

[8] Similarly, during the TOGA-COARE campaign *Wada et al.* [1999] conducted a study of equatorial inertia-gravity

[1]Department of Atmospheric and Oceanic Sciences, University of Colorado, Boulder, Colorado, USA.
[2]Colorado Research Associates, Division of NorthWest Research Associates, Boulder, Colorado, USA.

0148-0227/08/2007JD009289$09.00

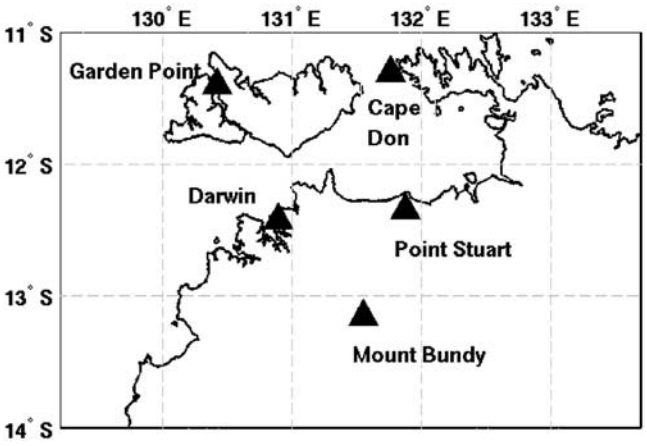

Figure 1. Location of the radiosonde sites used in the study.

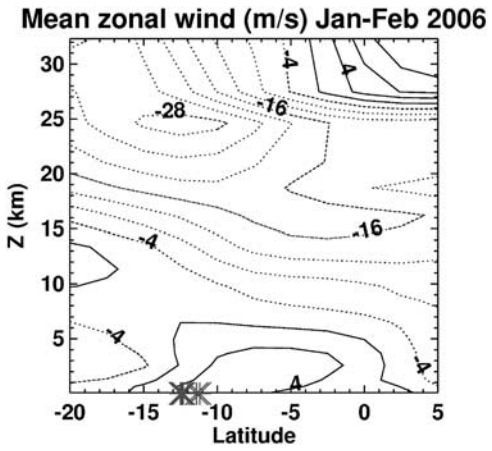

Figure 2. Latitude-height cross section of zonal wind averaged over January–February 2006 at the longitude of Darwin (130.89°) (from NCEP/DOE 2 Reanalysis data provided by the NOAA/OAR/ESRL PSD, Boulder, Colorado, USA, http://www.cdc.noaa.gov/). The contour interval is 4 ms^{-1}. Negative values are dotted. The crosses indicate the latitudes of the different radiosonde sites.

waves over the Western Pacific while the QBO was in the westerly shear phase. Two-day disturbances were observed in the lower stratosphere with vertical wavelengths of 3 to 5 km and horizontal wavelengths of several to ten thousand kilometers. The waves propagated eastward in the stratospheric westerlies.

[9] Recently, *Ratnam et al.* [2006] have shown evidence for inertia-gravity waves in the upper troposphere and lower stratosphere regions over Indonesia using CPEA campaign radiosonde data. The dominant gravity waves observed had a period of 2 to 3 d, a vertical wavelength of 3 to 5 km and a horizontal wavelength of 1700 km with a southeastward propagation. At that time the QBO was in the westerly phase. Observations of the different experiments indicate large-scale inertia-gravity waves with a propagation correlated to the phase of the QBO [*Baldwin et al.*, 2001]. Results of such studies are used to document the space-time variability of the wave-activity and hence improve the wave-drag parameterizations in climate models.

[10] In tropical Australia, the area of Darwin constitutes an ideal site to study convection as this region is under the influence of the Asian and Indian monsoons. In addition, both maritime and continental convective conditions occur. Therefore the Tropical Warm Pool International Cloud Experiment (TWP-ICE) was conducted from 23 January to 13 February 2006 in this area. The experiment goal was to describe the evolution of tropical convection, including the large-scale heat, moisture, and momentum budgets, while at the same time obtaining detailed observations of cloud properties and the impact of clouds on the environment. A general description of the campaign was given in the work of *May et al.* [2008].

Table 1. Radiosonde Profile Statistics

Sites	Total	$H > 20$ km	$H > 25$ km
Garden Point	162	62%	60%
Cape Don	173	72%	68%
Mount Bundy	165	78%	70%
Point Stuart	175	84%	73%
Darwin	82	90%	83%
Total	757	77.2%	70.8%

[11] Using TWP-ICE radiosonde data, we will focus in this paper on the study of 2-day (2-d) tropical waves observed during the campaign. The paper is organized as follows. The data and method used are described in section 2. The inferred wave properties are presented in section 3. Finally, section 4 discusses the nature of the waves and conclusions are given in section 5.

2. Method

2.1. Data

[12] The data used in this study are radiosonde data acquired eight times per day (3-hourly) from a circular network of four stations around Darwin (Figure 1) and from a ship west of Darwin. Contrary to the other sites Darwin has 6-hourly soundings. Table 1 presents the radiosonde profile statistics. On average more than 60% of the profiles reached an altitude of 28 km. In general in the first part of the campaign more profiles failed to reach 20 km. Point Stuart and Darwin had the largest percentage of balloons reaching 25 km. The ship was the site with the lowest profiles and therefore is not used in this study.

[13] The data are interpolated to a vertical spacing of 50m and additional interpolation in time is computed to fill the missing data. Temporal linear trends are then removed from the entire record to define the time series of perturbations of horizontal velocities and temperature.

2.2. Meteorological Conditions

[14] Figure 2 shows the latitude-height cross section of zonal wind averaged over January–February 2006 at the longitude of Darwin (130.89°E). The data correspond to the National Centers for Environmental Prediction reanalysis with 27 pressure levels. Between 20 and 25 km, easterly winds dominate with a westerly shear zone above: the

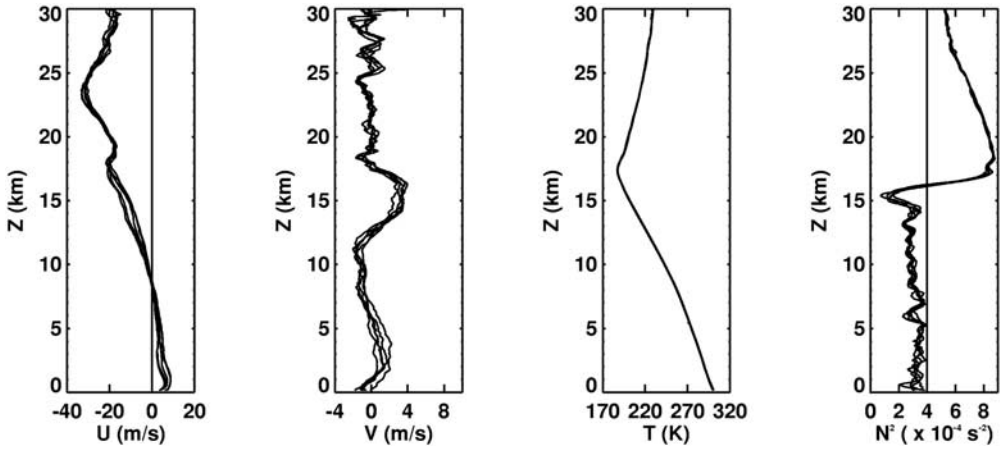

Figure 3. Mean vertical profiles of zonal wind (U), meridional wind (V), temperature (T), and buoyancy frequency squared (N^2) averaged over the TWP-ICE campaign period. Each line represents a different site.

transition from the end of the easterly phase to the beginning of the westerly phase of the QBO can be observed (Figure 2).

[15] The mean vertical profiles of zonal wind, meridional wind, temperature and buoyancy frequency squared averaged over the TWP-ICE campaign period are plotted on Figure 3. Weak westerlies below 5 km associated with the Australian monsoon were observed at all sites. The meridional wind was fairly weak with the presence of wave-like perturbations with growing amplitude above 20 km (Figure 3).

[16] During the experiment, the mean tropopause defined as the cold point tropopause was located at 17.5 km with a temperature of 190K and the buoyancy frequency N was equal to $2.4 \times 10^{-2}\mathrm{s}^{-1}$ in the stratosphere.

[17] At the beginning of the campaign, the Darwin area experienced an active monsoon. Figure 4 corresponds to a sequence of daily average (average over UTC times) infrared brightness temperature from 20 January to 31 January 2006. From 19 to 24 January Tropical Cyclone Daryl formed off the West Australia coast (around 18°S, 116°E) then moved southwest and weakened over the Indian Ocean (Figure 4). On 23 January a large Mesoscale Convective System developed south of Darwin (around 11°S, 128°E) and evolved into a large Mesoscale Convective Complex with an anvil exceeding 500 km in diameter. During the following days, the system moved over land and became a monsoon low. This monsoon low was observed until 1 February when it started to weaken. Break period conditions of the Australian monsoon were observed from 3 February until the end of the campaign.

2.3. Wavelet Analysis: S-Transform

[18] The S-Transform is used to analyze the time series of the perturbations. The S-Transform [*Stockwell et al.*, 1996] is a continuous wavelet transform analysis whose wavelet functions consist of sinusoidal functions modulated by a Gaussian. The width of the Gaussian window is proportional to the inverse of the frequency. During the analysis, only the Gaussian window is translated in time providing absolute phase information of the signal.

[19] Furthermore the S-Transform provides an accurate tool to estimate the phase lag between two time series $f_1(t)$ and $f_2(t)$ by means of the cross S-Transform which is defined as:

$$CrossST(t,f) = S_{f_1}(t,f)\left\{S_{f_2}(t,f)\right\}^* \quad (1)$$

$\{S_{f2}(t,f)\}^*$ is the complex conjugate of $S_{f2}(t,f)$. From the the cross-spectrum we can define the phase and covariance amplitude spectrum as:

$$\Phi(t,f) = \arctan\left[\frac{\Im(CrossST(t,f))}{\Re(CrossST(t,f))}\right] \quad (2)$$

$$Cov(t,f) = |CrossST(t,f)| \quad (3)$$

[20] The maximum of the covariance amplitude spectrum provides the amplitude and the frequency of the perturbation present in both signals. The phase at the frequency where the covariance is significant corresponds to the phase shift between the two time series.

[21] Previous studies have used the S-Transform for wave analysis. *Wang et al.* [2005] derived properties of small-scale gravity waves in winds and temperature measurements during the CRYSTAL-FACE campaign. More recently, *Alexander et al.* [2008] provided global estimates of gravity wave momentum flux from High Resolution Dynamics Limb Sounder (HIRDLS) observations.

3. Wave Properties

3.1. Period

[22] Figure 5 shows the time-height series of unfiltered perturbations of temperature, meridional and zonal winds observed at Point Stuart. Clear signatures of waves can be observed in the upper troposphere and stratosphere with downward phase propagation. The phase tilt indicates that

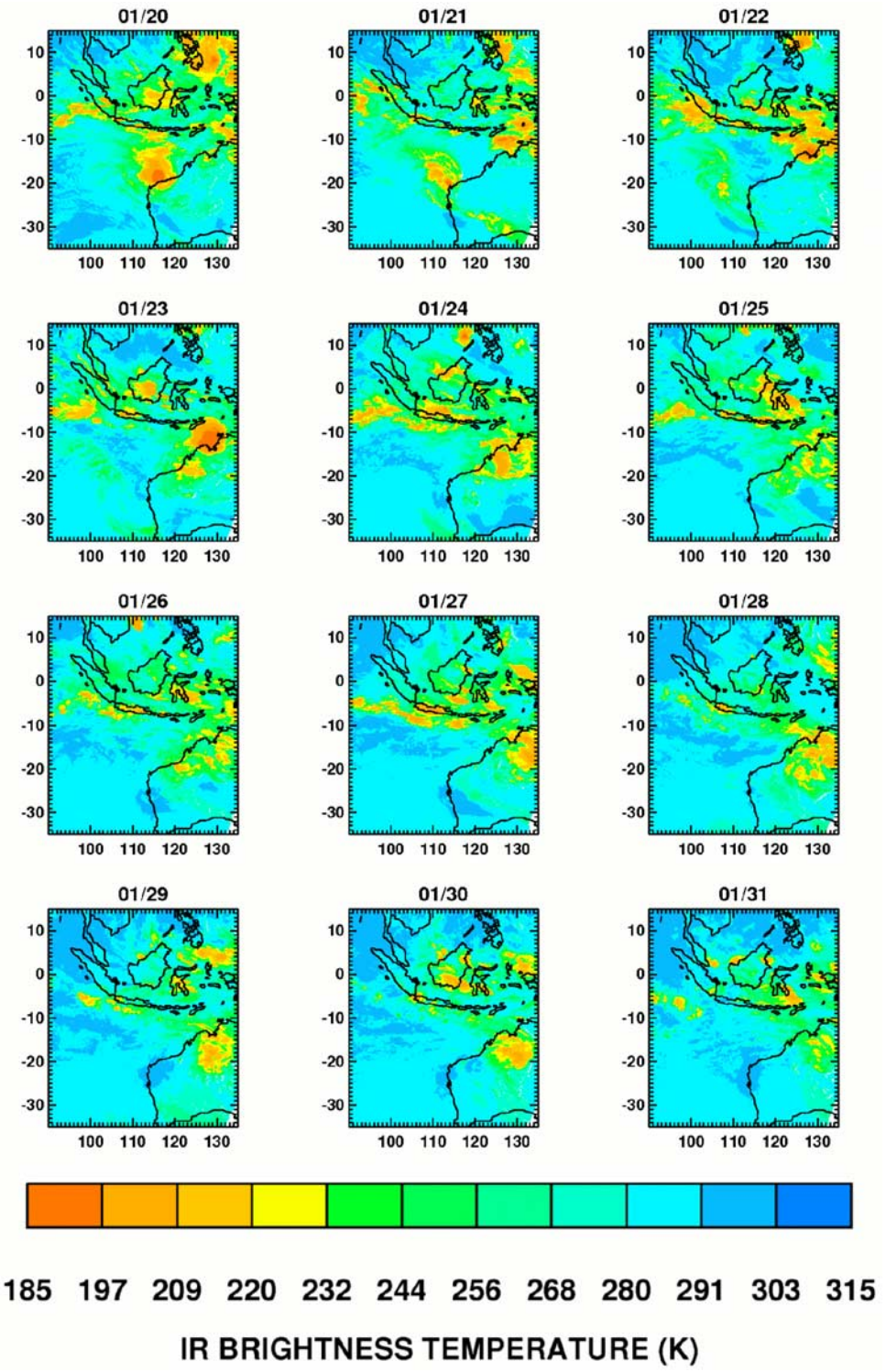

Figure 4. Sequence of daily average (average over UTC times) infrared brightness temperature (from TRMM global-merged data set) from 20 January to 31 January 2006. On 19 January Tropical Cyclone Daryl can be observed at 18°S, 116°E. On 23 January a Mesoscale Convective System developed south of Darwin (around 11°S, 128°E).

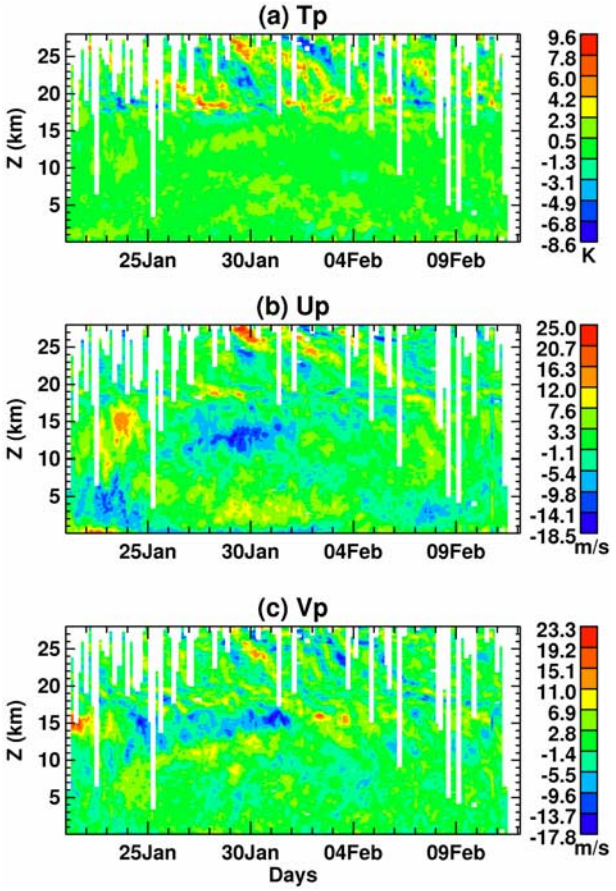

Figure 5. Time-height series of unfiltered perturbations of (a) Temperature (Tp), (b) zonal wind (Up), and (c) meridional wind (Vp) observed at Point Stuart.

energy is propagating upward. At 15 km, strong perturbations during the first 15 d of the campaign can be observed. The same features were observed at all the different sites (not shown). It is noteworthy that a diurnal tide was also observed in the data of temperature, zonal and meridional winds for all of the sites [*Alexander and Tsuda*, 2008].

[23] Figure 6 shows the average of the wavelet power spectra of time series of perturbations for the height ranges 22–26 km. The maximum amplitude corresponds to a period of 2.5 d for a wave event occuring in the middle of the campaign. Although at the latitude of Darwin, the inertial period is 2.4 d (corresponding to the longest period a gravity wave can have in this region), a signal with a period of 2.5 d can still be observed in the data, as 2.4 d refers to the longest intrinsic period while what is measured is the period in the ground-based reference frame. In order to remove longer period equatorial wave mode signals in the data and to keep the 2.5-d signal we apply a band-pass filter (a modified Welch window) with cut-off frequencies at 0.3 and 0.6 d^{-1} (1.7–3.3 d). The resulting filtered perturbations for Point Stuart can be seen on Figure 7.

3.2. Vertical Wavelength

[24] The difference of phase between the perturbations at various levels and a reference level can provide information about the vertical structure of the waves [*Wada et al.*, 1999].

[25] We use the cross-spectrum for a time series of zonal wind perturbations at a reference height and at other different altitudes. The reference height is fixed at 23 km which corresponds to the altitude of maximum amplitude for the 2.5 d-period. The vertical profiles of phase differences and coherences of the zonal wind perturbations u' for a period of 2.5 d can be seen on Figure 8. A consistent phase-height relationship is observed above 20 km associated with a strong coherence. From the profile of phase difference the vertical wavelength is estimated to be around 6 km for the zonal wind perturbations. The analysis for the meridional wind perturbations gives a similar result (not shown). The temperature fluctuations show a vertical wavelength in the range 5–7 km and somewhat higher variability is observed in the phase and coherence (not shown).

3.3. Horizontal Structure

[26] For each altitude between 22 and 26 km the phase shift between two sites is calculated by averaging over the

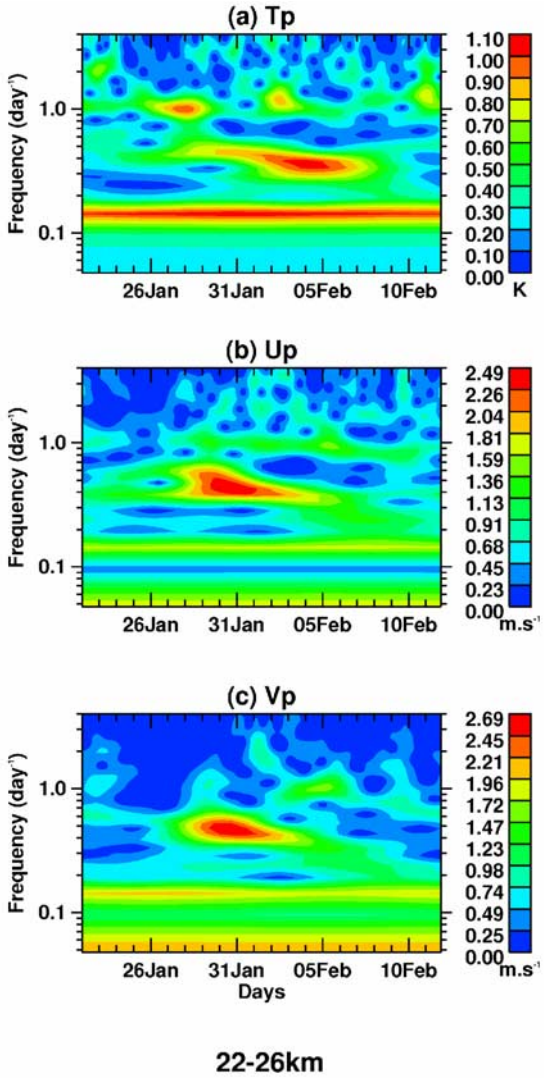

Figure 6. Time-frequency spectrum averaged between 22 and 26 km for the perturbations of (a) temperature, (b) zonal wind, and (c) meridional wind observed at Point Stuart.

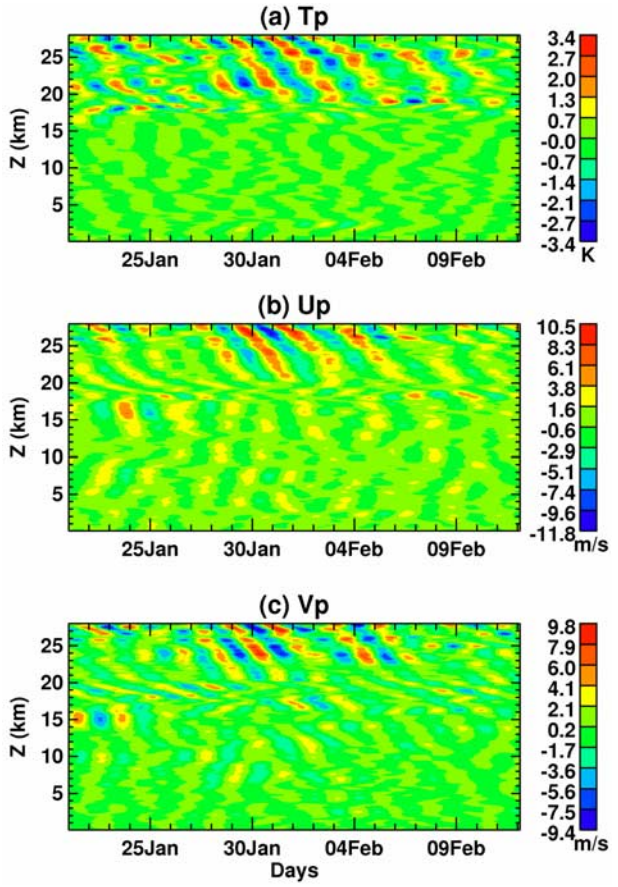

Figure 7. Time-height series showing the perturbations of (a) temperature (Tp), (b) zonal wind (Up), and (c) meridional wind (Vp) observed in the 1.7–3 d range at Point Stuart.

2-d time period surrounding the maximum in the wavelet covariance spectrum (defined by the frequency f_m and time t_m). The final phase shift between two sites is the average of the vertical profile of phase between 21 and 26 km.

[27] From the horizontal phase lag, the apparent wavelength is estimated along the line joining the two sites by:

$$\lambda_a = \frac{2\pi\Delta x}{\Delta\phi} \tag{4}$$

Where Δx is the distance between the two sites.

[28] Figure 9 presents the vertical profiles of phase differences for time series of zonal wind between Mount Bundy and the other sites. On this plot, Mount Bundy is taken as the reference site. The same calculations were done for Point Stuart and the average phase differences are summarized in Table 2 and Table 3. The values of phase differences show that Mount Bundy lags Point Stuart which lags Cape Don and Garden Point. This fact indicates a south to southeastward propagation for the waves. For finding the horizontal wavelength, we compute an angle of propagation and a horizontal wavelength that fits the apparent horizontal wavelengths along the lines joining pairs of sites [*Ratnam et al.*, 2006]. Considering lines of constant phase of the wave on an (x, y) plane, if the line between two sites lies along the propagation direction of the wave, then the true horizontal wavelength is equal to the apparent horizontal wavelength. If the line between two sites lies at different angles α_1 and α_2 from the propagation direction (Figure 10) then:

$$\lambda_h = \lambda_1 \cos\alpha_1 = \lambda_2 \cos\alpha_2 \tag{5}$$

[29] In this equation, λ_h is the true horizontal wavelength, λ_1 and λ_2 are the apparent wavelengths between site 1 and site 2 and between site 1 and site 3 respectively. Using these equations for each pair of sites, a combination of three sites gives the solution:

$$\delta = \arctan\left(\frac{\lambda_2\cos\theta_2 - \lambda_1\cos\theta_1}{\lambda_1\sin\theta_1 - \lambda_2\sin\theta_2}\right) \tag{6}$$

[30] Where δ is the horizontal angle of propagation (expressed in degree from the West-East direction). The values of apparent wavelengths found between the different pairs of sites are given in Table 4 and the angles of propagation and horizontal wavelengths found using (5) and (6) are presented in Table 5. We found a mean horizontal wavelength of 7220 km (5500 to 8700 km) and an angle of propagation of $-74°$ (in degrees from the eastward direction).

[31] In addition we computed the mean direction of propagation by using the covariance between the velocities and temperature perturbations. The mean direction (in degrees from the eastward direction) can be expressed as [*Vincent et al.*, 1997]:

$$\delta = \arctan\left(\frac{\overline{u' T'_{+90}}}{\overline{v' T'_{+90}}}\right) \tag{7}$$

[32] Where T'_{+90} is the value of the temperature after shifting the phase by $+90°$ via the Hilbert transform.

[33] Figure 11 shows the distribution of the mean direction of propagation for all of the sites. 63% of the profiles show a southeastward propagation ($-90° < \delta < 0°$). For angles less than 0 degree (southward propagation), the median is $-47.3°$ which is consistent with the southeastward propagation established with the cross-spectrum analysis.

4. Identification of Inertia-Gravity Waves

4.1. Quadrature Spectrum

[34] Inertia-gravity waves are influenced by the rotation of the Earth and have intrinsic frequencies of the same order as the Coriolis parameter. For these types of waves, the wind velocity perturbations are related by *Fritts and Alexander* [2003]:

$$\tilde{v} = -i\frac{f}{\hat{\omega}}\tilde{u} \tag{8}$$

where $\tilde{u}$ and $\tilde{v}$ correspond to the amplitudes of the wind velocity perturbations that are parallel and orthogonal to the wave propagation direction respectively. The wind velocity

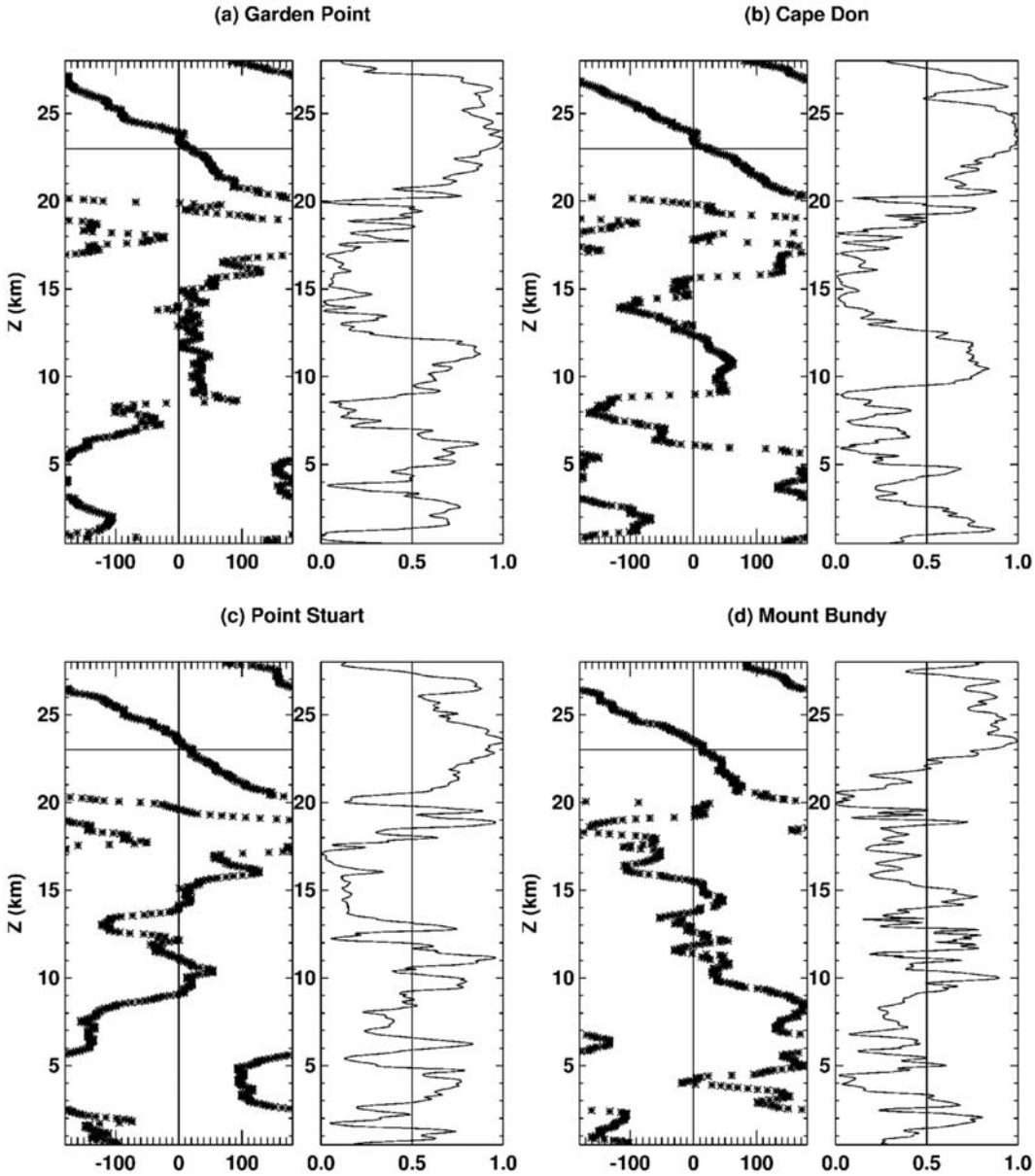

Figure 8. Vertical profiles of phase differences and coherences of u for a period of 2.5 d at (a) Garden Point, (b) Cape Don, (c) Point Stuart, and (d) Mount Bundy. The reference level is 23 km.

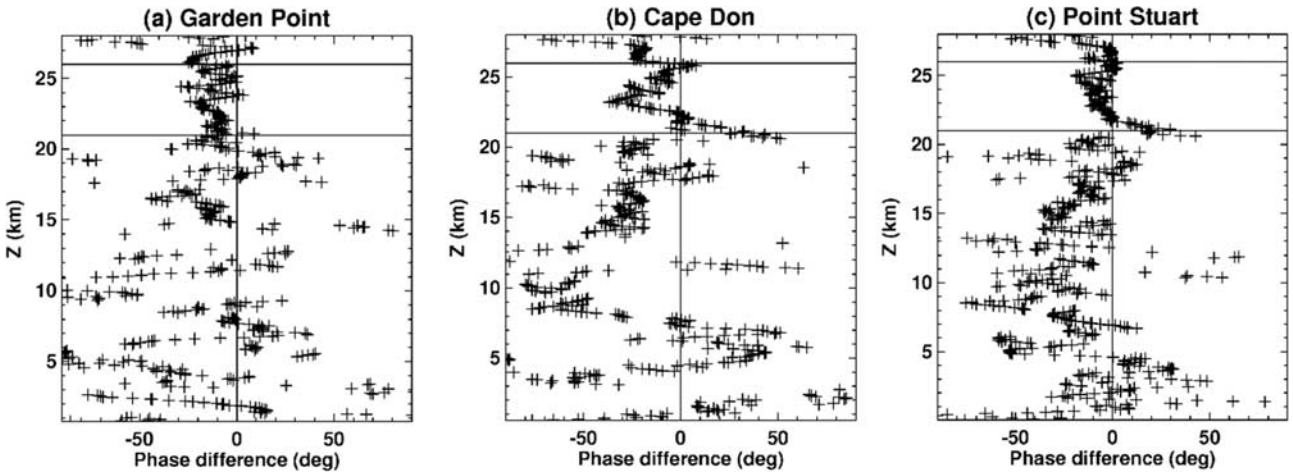

Figure 9. Vertical profiles of phase differences for time series of zonal wind between (a) Mount Bundy and Garden Point, (b) Mount Boundy and Cape Don, and (c) Mount Bundy and Point Stuart.

perturbations are one-quarter cycle out of phase, and thus will have large signals in the quadrature spectrum of zonal (u') and meridional (v') wind fluctuations. Figure 12 shows the vertical profile of the quadrature spectrum of u' and v'. Large amplitudes can be seen above 22 km demonstrating the presence of inertia-gravity waves during the campaign in the lower stratosphere.

4.2. Intrinsic Frequency and Group Propagation

[35] To assess the wave characteristics relevant to the general circulation, we can use the dispersion relation for low frequency inertia-gravity waves. For a linear gravity wave with horizontal wave number k_h,

$$\hat{\omega} = \omega - \bar{u_h} k_h, \tag{9}$$

where ω is the ground-based frequency and $\bar{u_h}$ is the background wind speed in the direction of wave propagation. During the campaign, the background wind was easterly in the stratosphere (-25 ms^{-1}). Assuming that the waves propagate southeastward toward $-74°$, have a ground-based period of 2.5 d, a horizontal wavelength λ_h around 5500 to 8700 km, the intrinsic frequency is estimated to be around 3.70×10^{-5}s^{-1} and 3.41×10^{-5}s^{-1} ($\approx$ 2 d).

[36] Furthermore, $\hat{\omega}$ can be deduced from the dispersion relation for low-frequency inertia-gravity waves [*Fritts and Alexander*, 2003]:

$$\hat{\omega}^2 = f^2 + N^2 \frac{k_h^2}{m^2} \tag{10}$$

f represents the Coriolis parameter equal to -3.132×10^{-5}s^{-1} at the latitude of Darwin, N is the buoyancy frequency ($= 2.449 \times 10^{-2}$s^{-1} in the stratosphere), k_h and m are the horizontal and vertical wave numbers. According to equation (10) $\hat{\omega}$ is equal to 4.12×10^{-5}s^{-1} and 3.56×10^{-5}s^{-1} for λ_h equal to 5500 km and 8700 km respectively. In both cases, the relative error is less than 11% which confirms the estimate of the wave parameters.

[37] The vertical group velocity ($-\frac{k_h^2 N^2}{\hat{\omega} m^3}$) lies between 1.62 km/d and 0.647 km/d for λ_h between 5500 and 8700 km. Assuming a source located in the troposphere (convection) and waves generated in the upper troposphere around 17 km, then 4 to 12 d are needed for the perturbations to propagate upward to 25 km. The S-Transform analysis indicates that the wave mainly occurred between the 28 January and the 5 February. Using a vertical profile of temperature averaged over the campaign period we can estimate $\tau(m, z)$, the scale-dependent relaxation time for radiative damping [*Fels*, 1982]. Figure 13 shows the vertical profile of $\tau(m, z)$ for a vertical wavelength of 6 km. Between 20 and 28 km the average $\tau(m, z)$ is equal to 6.7 d. This value is in agreement with the time observed for the wave to dissipate in the stratosphere and suggests that radiative damping is the main cause of the wave attenuation.

[38] On Figure 4, the low values of brightness temperature over the Indonesian region tend to indicate strong convective activity on the middle of January. For low frequency inertia-gravity waves the vertical group velocity is much smaller than the horizontal group velocity. Therefore this type of wave can propagate over large horizontal distances and the observed wave is likely generated in association with strong convection over Indonesia.

[39] These waves cannot propagate meridionally beyond the latitude at which the intrinsic wave frequency equals the

Table 2. Phase Differences Between Mount Bundy and Other Sites[a]

Sites	Phase Difference, deg	Distance, km	λ_a, km
Garden Point	−10.56	230.26	7850
Cape Don	−8.38	206.35	8865
Point Stuart	−2.85	96.62	12,205

[a]Mount Bundy is taken as the reference site.

Table 3. Phase Differences Between Point Stuart and Other Sites[a]

Sites	Phase Difference, deg	Distance, km	λ_a, km
Garden Point	−7.63	190.51	8989
Cape Don	−6.20	115.92	6731

[a]Point Stuart is taken as the reference site.

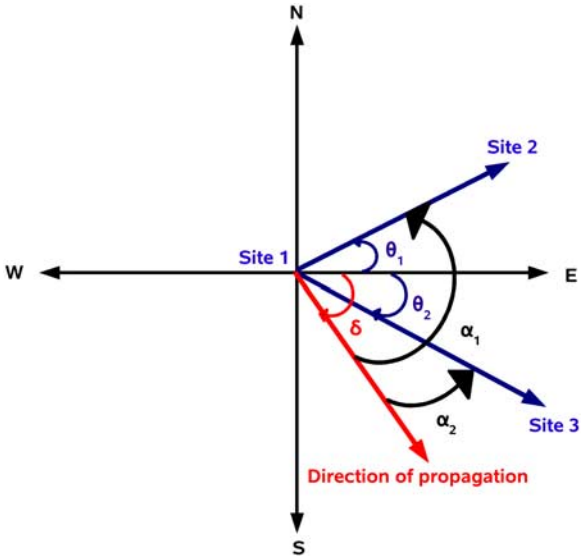

Figure 10. Schematic showing angles between sites (see text for explanations).

inertial frequency [*Sato et al.*, 1999, 2003] and with $\hat{\omega} = 3.64 \times 10^{-5}\mathrm{s}^{-1}$ (period of 2 d) the critical latitude corresponds to ± 14.44°. The waves observed may be refracted or absorbed while moving southward toward the critical latitude. After refraction if they still propagate upward and eastward in the equatorial region they might encounter the westerly wind observed at 6°S on Figure 2. This can cause the vertical wavelength to shrink and thus to decrease the scale-dependent relaxation time for radiative damping. As a result the dissipation might be stronger after refraction at 14.44°S.

[40] The latitudinal distribution of the QBO in the zonal wind has a 12° half-width and considerable amplitudes are still observed at 20° [*Baldwin et al.*, 2001]. Thus the calculated critical latitudes are well inside the QBO region and the observed wave might impact the mean circulation between ±14.44°.

4.3. Wave Energy

[41] According to the linear wave theory, the partitioning of total gravity wave energy into potential energy (PE) and kinetic energy (KE) depends on the ratio $\alpha = \frac{|k_h|}{|m|}$ [*Gill*, 1982]:

$$\frac{KE}{PE} = 1 + \frac{2f^2}{N^2\alpha^2} \tag{11}$$

[42] *Yamamori and Sato* [2006] used the dispersion relation for low frequency inertia-gravity waves to express (11) as:

$$\frac{KE}{PE} = \frac{1 + (f/\hat{\omega})^2}{1 - (f/\hat{\omega})^2} \tag{12}$$

[43] For the area of Darwin f varies between $-3.338 \times 10^{-5}\mathrm{s}^{-1}$ (at Cape Don) and $-3.073 \times 10^{-5}\mathrm{s}^{-1}$ (at Mount Bundy) which gives a mean value of $-3.205 \times 10^{-5}\mathrm{s}^{-1}$. With an intrinsic period of 2 d then KE/PE should equal 6. We compute the mean kinetic and potential energies for the period corresponding to the maximum of wave activity between 28 January and 5 February. The mean temperature and buoyancy profiles used to define PE were estimated by an average over the period of the campaign. Table 6 shows the averaged potential and kinetic energies as well as the ratio of KE to PE for the band-pass filtered perturbations for the height ranges 22–27 km. In general a mean ratio between five and six was observed for all the sites except Darwin. As expected, the large ratio for KE/PE is consistent with the presence of low-frequency inertia-gravity waves in the stratosphere.

4.4. Momentum Flux

[44] To assess the importance of the wave event we compute the total vertical flux of horizontal momentum associated with the 2-d waves,

$$F_{ph} = \bar{\rho}\left(1 - \frac{f^2}{\hat{\omega}^2}\right)\left(\overline{u'w'}^2 + \overline{v'w'}^2\right)^{1/2} \tag{13}$$

Ern et al. [2004] expressed equation (13) as,

$$F_{ph} = \left[1 - \frac{\hat{\omega}^2}{N^2}\right]\left[1 + \frac{1}{m^2}\left(\frac{1}{2H} - \frac{g}{c_s^2}\right)\right]^{-1} \times \left[1 + \left(\frac{f}{\hat{\omega}m}\right)^2\left(\frac{1}{2H} - \frac{g}{c_s^2}\right)\right]^{1/2} \times \frac{1}{2}\bar{\rho}\frac{k_h}{m}\left(\frac{g}{N}\right)^2\left(\frac{\hat{T}}{\overline{T}}\right)^2 \tag{14}$$

where $\hat{T}$ is the temperature amplitude of the wave, k_h and m are the horizontal and vertical wave numbers, $\bar{\rho}$ is the background density, g is Earth's gravitational acceleration, N is the buoyancy frequency, H is the scale height of the atmosphere and $\overline{T}$ is the background temperature. As $\hat{\omega} \ll N$ and $1/\mathrm{m}^2 \ll 4\mathrm{H}^2$, by letting the sound speed $c_s \to \infty$ (14) yields:

$$\frac{F_{ph}}{\bar{\rho}} = \frac{1}{2}\frac{k_h}{m}\left(\frac{g}{N}\right)^2\left(\frac{\hat{T}}{\overline{T}}\right)^2 \tag{15}$$

Table 4. Apparent Wavelengths Between the Different Pairs of Sites (G: Garden Point, C: Cape Don, P: Point Stuart, M: Mount Bundy)

λ, km	G	C	P	M
G	0			
C	180,000	0		
P	8989	6731	0	
M	7850	8865	12205	0

Table 5. Directions of Horizontal Propagation (Degrees From East) Estimated With Different Combinations of Sites

	GCP	PGC	CPG	GPM	PMC	MGP	CPM	GCM	CMG	MGC	Average
Angle, deg	−86	−86	−76	−62	−61	−63	−66	−86	−67	−86	−74
λ, km	6727	5475	6661	7900	7832	7817	6411	8715	7741	6919	7220

[45] With a mean stratospheric temperature of $\overline{T}$ = 217K between 20 and 30 km, $\hat{T}$ = 1.10K estimated with the S-Transform analysis, for λ_h between 5500 and 8700 km, λ_z = 6 km then $F_{ph}/\bar{\rho}$ is ranging from 1.4 × 10^{-3} to 2.2 × 10^{-3}m^{2}s^{-2}.

[46] The vertical flux of horizontal momentum obtained with (15) corresponds to an absolute value and thus does not take in account the wave propagation direction. However, *Sato and Dunkerton* [1997] used the quadrature spectra Q_{Tu} of u and T fluctuations to provide a direct estimate of the zonal momentum flux of equatorial waves. By analogy, the total momentum flux in the horizontal direction of propagation of the wave can be expressed as,

$$\overline{u_h' w'} = -\frac{g}{\overline{T}N^2}\int_{\omega_1}^{\omega_2} Q_{Tu_h}(\hat{\omega})\hat{\omega}d\hat{\omega} \tag{16}$$

where Q_{Tu_h} is the quadrature spectrum of T and u_h, the wind fluctuations along the horizontal direction of propagation. The quadrature spectrum is calculated for both propagation directions (−74° and −47.3°) for all stations considered. First $Q_{Tu_h}(\omega)$, the quadrature spectrum as a function of the ground-based frequency, is computed by using the cross S-Transform of T and u_h series at each altitude. The result is then averaged for the period of maximum wave activity between 28 January and 5 February. Then $Q_{Tu_h}(\omega)$ is shifted by 0.5 d (which corresponds to the average difference between intrinsic and ground-based wave periods) to obtain the quadrature spectrum as a function of the intrinsic frequency $Q_{Tu_h}(\hat{\omega})$. Finally $Q_{Tu_h}(\hat{\omega})$ at each altitude is integrated between the frequencies 0.4 and 0.7 d^{-1} (1.5–2.5 d) to make sure that the 2-d spectral peak attributed to the inertia-gravity wave is covered. We use 217 K and 6 × 10^{-4}s^{-2} as values for $\overline{T}$ and N^2.

[47] Figure 14 shows the vertical profiles of momentum flux for waves of 1.5–2.5 d period for all of the sites for both propagation directions. For all the sites positive values of $\overline{u_h' w'}$ were observed above 20 km. This confirms the dominance of an upward and southeastward propagating wave in the range 0.4–0.7 d^{-1}. The momentum flux starts to decrease above 25 km. As the winds are easterly in the stratosphere and the waves propagate eastward, the observed waves are not attenuated because of the critical-level effect.

[48] Moreover, we have previously seen that the radiative damping is probably the main process responsible for the waves attenuation between 20 and 28 km. This agrees with the fact that the maximum of momentum flux is seen at 25 km.

[49] Table 7 summarizes the average of $\overline{u_h' w'}$ for the height region 20 to 28 km at each station. Values of total momentum flux $\overline{u_h' w'}$ and zonal momentum flux $\overline{u'w'}$ are shown for the two different angles of propagation. The values of total momentum fluxes obtained from (15) and (16) are of the same order of magnitude and range from 1 to 2 × 10^{-3} m^{2}s^{-2}.

[50] The uncertainty in the direction of propagation leads to an uncertainty in the values of the zonal momentum fluxes. We can see that the average of $\overline{u'w'}$ between 20 and 28 km ranges from 0.3 to 1.03 × 10^{-3} m^{2}s^{-2}.

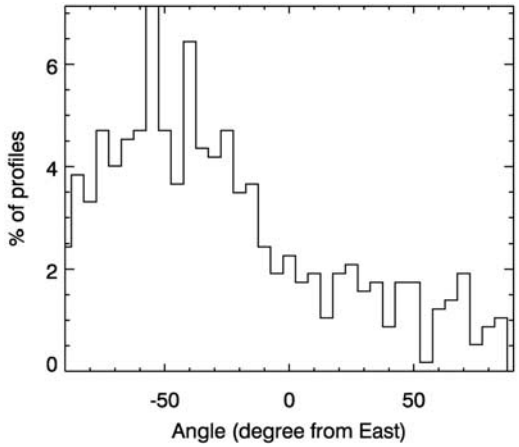

Figure 11. Distribution of directions of horizontal propagation derived from velocity and temperature perturbations. The distribution includes angles for Garden Point, Mount Bundy, Point Stuart, and Cape Don.

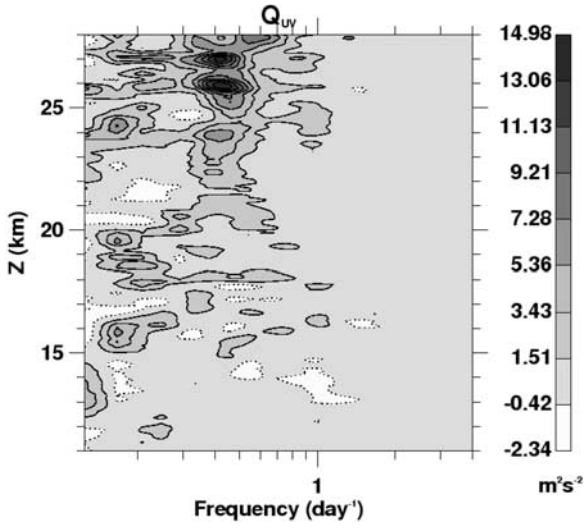

Figure 12. Vertical profile of quadrature spectrum of zonal and meridional wind perturbations observed at Garden Point. Positive quadrature in solid and negative quadrature in dots.

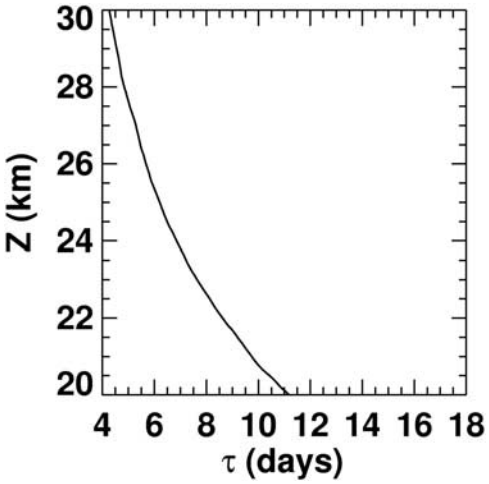

Figure 13. Vertical profile of timescale for radiative damping for a vertical wavelength of 6 km.

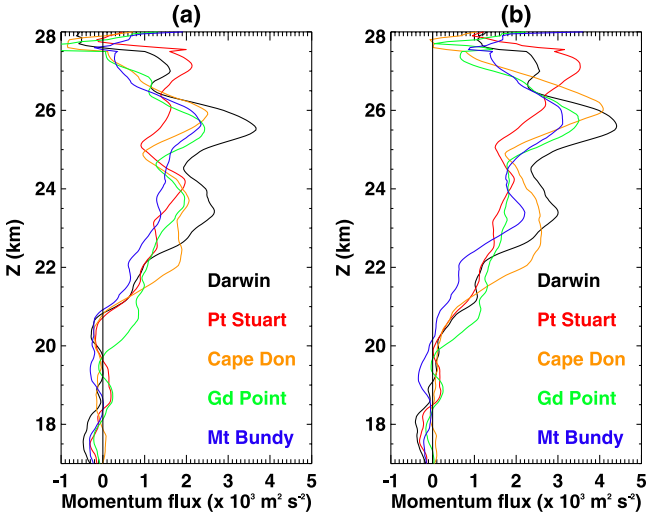

Figure 14. Vertical profiles of the momentum fluxes for waves of 1.5–2.5 d period for all of the sites. (a) Angle of propagation of −74° and (b) angle of propagation of −47.3°.

[51] The upper limit of $\overline{u'w'}$ is consistent with the values of momentum fluxes obtained by Sato and Dunkerton for 1–3 d waves during the easterly shear phase of the QBO at Singapore (1.4°N, 104°E). In addition, the zonal momentum fluxes observed are greater than those obtained by *Holton et al.* [2001] for 8–17 and 4–6 d Kelvin waves at Nauru (0.5°S, 166.9°E) and *Murthy et al.* [2002] for 6.7 and 7.8 d Kelvin waves observed at Gadanki (13.5°N, 79.2°E).

5. Conclusions

[52] A 2-d wave event was observed during the TWP-ICE campaign, from 28 January to 5 February in the lower stratosphere over the Darwin area. Using the S-Transform analysis, the vertical and horizontal wavelengths were estimated to be around 6 km and 7220 km respectively. Moreover, the waves showed a southeastward propagation confirmed both by the cross S-Transform analysis and the covariance of horizontal velocities and temperature fluctuations. The group velocity of the observed waves being small, they were confined to the lower stratosphere and were likely attenuated because of radiative damping. The waves were identified as low frequency inertia-gravity waves as shown by the consistency between the inferred wave parameters and the dispersion relation for low frequency inertia-gravity waves. The ratio of KE to PE in the lower stratosphere is also in agreement with the linear wave theory. Additionally, the momentum flux associated with the waves was estimated by two methods. A first value of total vertical momentum flux of 1.4×10^{-3} to 2.2×10^{-3} m^2 s^{-2} was found using Ern et al's estimate. The second estimate is based on the quadrature spectra of u_h' and T', giving values of total momentum flux in the range 1×10^{-3} to 2.16×10^{-3} m^{2}s^{-2}. Both estimates are consistent. The corresponding values of zonal momentum flux found are of the same order as values of zonal momentum flux associated with Kelvin waves and thus constitute evidence for the importance of forcing of the tropical circulation by intermediate-scale inertia-gravity waves. At the moment, in the General Circulation Models (GCMs), an emphasis is placed on the simulations of the largest planetary-scale waves and parametrization of the small-scale gravity waves. The contribution of intermediate scale waves is often neglected. However, many current GCMs have sufficient horizontal resolution to resolve these intermediate-scale waves. This study shows that a climatology of intermediate-scale wave parameters determined from measurements is essential to validate the results of high resolution GCMs.

[53] Owing to the development of high-resolution satellites like AIRS (Atmospheric Infrared Sounder) and HIRDLS (High Resolution Dynamics Limb Sounder) global estimates of momentum flux can now be derived. In addition, we need to understand the link between convection and the intermediate scale waves. Modeling is needed to assess the sources

Table 6. Density of Kinetic (KE) and Potential Energy (PE) Averaged Between 22 and 27 km for All of the Sites

Sites	KE, m^{2}s^{-2}	PE, m^{2}s^{-2}	KE/PE
Garden Point	14.2	2.6	5.5
Cape Don	18.7	3.2	5.8
Point Stuart	13.5	2.5	5.4
Darwin	15.2	4.1	4.1
Mount Bundy	13.5	2.7	5.0

Table 7. Total Momentum Flux $\overline{u_h'w'}$ and Zonal Momentum Flux $\overline{u'w'}$ ($\times 10^{-3}$ m^{2}s^{-2}) Averaged Between 20 and 28 km

Sites	$\overline{u_h'w'}$ (−74°)	$\overline{u_h'w'}$ (−47.3°)	$\overline{u'w'}$ (−74°)	$\overline{u'w'}$ (−47.4°)
Garden Point	1.18	1.68	0.33	0.80
Cape Don	1.17	1.94	0.39	0.82
Point Stuart	1.14	1.69	0.31	0.78
Darwin	1.52	2.16	0.42	1.03
Mount Bundy	1.00	1.56	0.30	0.70

and mechanisms which lead to the generation of such waves.

[54] **Acknowledgments.** The authors wish to thank Kaoru Sato and Simon Alexander for constructive comments. This material is based upon work supported by the National Science Foundation under grant 0632378. Any opinions, findings, and conclusions or recommendations expressed in this material are those of the authors and do not necessarily reflect the views of the National Science Foundation.

References

Alexander, S. P., and T. Tsuda (2008), Observations of the diurnal tide during seven intensive radiosonde campaigns in Australia and Indonesia, *J. Geophys. Res.*, *113*, D04109, doi:10.1029/2007JD008717.

Alexander, M. J., et al. (2008), Global estimates of gravity wave momentum flux from High Resolution Dynamics Limb Sounder observations, *J. Geophys. Res.*, *113*, D15S18, doi:10.1029/2007JD008807.

Antonita, T. M., G. Ramkumar, K. K. Kumar, K. S. Appu, and K. V. S. Nambhoodiri (2007), A quantitative study on the role of gravity waves in driving the tropical Stratospheric Semiannual Oscillation, *J. Geophys. Res.*, *112*, D12115, doi:10.1029/2006JD008250.

Baldwin, M. P., et al. (2001), The quasi-biennial oscillation, *Rev. Geophys.*, *39*(2), 179–229.

Cadet, D., and H. Teitelbaum (1979), Observational evidence of internal inertia-gravity waves in the tropical stratosphere, *J. Atmos. Sci.*, *36*, 892–907.

Dunkerton, T. J. (1997), The role of gravity-waves in the quasi-biennial oscillation, *J. Geophys. Res.*, *102*(D22), 26,053–26,076.

Ern, M., P. Preusse, M. J. Alexander, and C. D. Warner (2004), Absolute values of gravity wave momentum flux derived from satellite data, *J. Geophys. Res.*, *109*, D20103, doi:10.1029/2004JD004752.

Fels, S. B. (1982), A parameterization of scale-dependent radiative damping rates in the middle atmosphere, *J. Atmos. Sci.*, *39*, 1141–1152.

Fritts, D. C., and M. J. Alexander (2003), Gravity wave dynamics and effects in the middle atmosphere, *Rev. Geophys.*, *41*(1), 1003, doi:10.1029/2001RG000106.

Gill, A. E. (1982), *Atmosphere-Ocean Dynamics*, p. 662, Elsevier, New York.

Holton, J. R., M. J. Alexander, and M. T. Boehm (2001), Evidence for short vertical wavelength Kelvin waves in the Department of Energy-Atmospheric Radiation Measurement Nauru99 radiosonde data, *J. Geophys. Res.*, *106*(D17), 20,125–20,129.

Lieberman, R. S., D. M. Riggin, R. R. Garcia, Q. Wu, and E. E. Remsberg (2006), Observations of intermediate-scale diurnal waves in the equatorial mesosphere and lower thermosphere, *J. Geophys. Res.*, *111*, A10S11, doi:10.1029/2005JA011498.

May, P. T., J. H. Mather, G. Vaughan, C. Jakob, G. M. McFarquhar, K. N. Bower, and G. G. Mace (2008), The tropical warm pool international cloud experiment, *Bull. Am. Meteorol. Soc.*, *89*, 629–645.

Murthy, B. V. K., K. Satheesan, K. Parameswaran, M. N. Sasi, G. Ramkumar, Y. Bhavanikumar, K. Raghunath, and M. Krishniah (2002), Equatorial waves in temperature in the altitude range 4 to 70 km, *Q. J. R. Meteorol. Soc.*, *128*(581), 819–837.

Plumb, R. A. (1984), The quasi-biennial oscillation, in *Dynamics of the Middle Atmosphere*, edited by J. R. Holton and T. Matsuno, pp. 217–251, Terra Sci., Tokyo.

Ratnam, M. V., T. Tsuda, Y. Shibagaki, T. Kozu, and S. Mori (2006), Gravity wave characteristics over the equator observed during the CPEA campaign using simultaneous data from multiple stations, *J. Meteorol. Soc. Jpn.*, *84A*, 239–257.

Sassi, F., and R. R. Garcia (1997), The role of equatorial waves forced by convection in the tropical semiannual oscillation, *J. Atmos. Sci.*, *54*, 1925–1942.

Sato, K., and T. J. Dunkerton (1997), Estimate of momentum flux associated with equatorial Kelvin and gravity waves, *J. Geophys. Res.*, *102*(D22), 26,247–26,261.

Sato, K., T. Kumakura, and M. Takahashi (1999), Gravity waves appearing in a high-resolution GCM simulation, *J. Atmos. Sci.*, *56*, 1005–1018.

Sato, K., M. Yamamori, S. Ogino, N. Takahashi, Y. Tomikawa, and T. Yamanouchi (2003), A meridional scan of the stratospheric gravity wave field over the ocean in 2001 (MeSSO2001), *J. Geophys. Res.*, *108*(D16), 4491, doi:10.1029/2002JD003219.

Stockwell, R. G., L. Mansinha, and R. P. Lowe (1996), Localisation of the complex spectrum: The S-transform, *IEEE*, *44*(4), 998–1001.

Vincent, R. A., S. J. Allen, and S. D. Eckermann (1997), Gravity-wave parameters in the lower stratosphere, in *Gravity Wave Processes: Their Parameterization in Global Climate Models*, edited by K. Hamilton, pp. 7–25, Springer, New York.

Wada, K., T. Nitta, and K. Sato (1999), Equatorial inertia-gravity waves in the lower stratosphere revealed by TOGA-COARE IOP data, *J. Meteorol. Soc. Jpn.*, *77*(3), 721–736.

Wang, L., M. J. Alexander, T. P. Bui, and M. J. Mahoney (2005), Small-scale gravity waves in ER-2 MMS/MTP wind and temperature measurements during CRYSTAL-FACE, *Atmos. Chem. Phys.*, *6*, 1091–1104.

Yamamori, M., and K. Sato (2006), Characteristics of inertia gravity waves over the South Pacific as revealed by radiosonde observations, *J. Geophys. Res.*, *111*, D16110, doi:10.1029/2005JD006861.

M. J. Alexander, Colorado Research Associates, Division of NorthWest Research Associates, 3380 Mitchell Lane, Boulder, CO 80301, USA.

S. Evan, Department of Atmospheric and Oceanic Sciences, UCB 311, University of Colorado, Boulder, CO 80309-0311, USA. (stephanie.evan@colorado.edu)